

The faster the narrower: characteristic bulk velocities and jet opening angles of Gamma Ray Bursts

G. Ghirlanda^{1*}, G. Ghisellini¹, R. Salvaterra², L. Nava³, D. Burlon⁴, G. Tagliaferri¹, S. Campana¹, P. D’Avanzo¹, A. Melandri¹

¹INAF – Osservatorio Astronomico di Brera, via E. Bianchi 46, I-23807 Merate, Italy

²INAF - IASF Milano, via E. Bassini 15, I-20133 Milano, Italy

³APC Université Paris Diderot, 10 rue Alice Domon et Leonie Duquet, F-75205 Paris Cedex 13, France

⁴Sydney Institute for Astronomy, School of Physics, The University of Sydney, NSW 2006, Australia

ABSTRACT

The jet opening angle θ_{jet} and the bulk Lorentz factor Γ_0 are crucial parameters for the computation of the energetics of Gamma Ray Bursts (GRBs). From the ~ 30 GRBs with measured θ_{jet} or Γ_0 it is known that: (i) the real energetic E_γ , obtained by correcting the isotropic equivalent energy E_{iso} for the collimation factor $\sim \theta_{\text{jet}}^2$, is clustered around 10^{50} – 10^{51} erg and it is correlated with the peak energy E_p of the prompt emission and (ii) the comoving frame E'_p and E'_γ are clustered around typical values. Current estimates of Γ_0 and θ_{jet} are based on incomplete data samples and their observed distributions could be subject to biases. Through a population synthesis code we investigate whether different assumed intrinsic distributions of Γ_0 and θ_{jet} can reproduce a set of observational constraints. Assuming that all bursts have the same E'_p and E'_γ in the comoving frame, we find that Γ_0 and θ_{jet} cannot be distributed as single power-laws. The best agreement between our simulation and the available data is obtained assuming (a) log-normal distributions for θ_{jet} and Γ_0 and (b) an intrinsic relation between the peak values of their distributions, i.e. $\theta_{\text{jet}}^{2.5}\Gamma_0 = \text{const}$. On average, larger values of Γ_0 (i.e. the “faster” bursts) correspond to smaller values of θ_{jet} (i.e. the “narrower”). We predict that $\sim 6\%$ of the bursts that point to us should not show any jet break in their afterglow light curve since they have $\sin \theta_{\text{jet}} < 1/\Gamma_0$. Finally, we estimate that the local rate of GRBs is $\sim 0.3\%$ of all local SN Ib/c and $\sim 4.3\%$ of local hypernovae, i.e. SN Ib/c with broad-lines.

Key words: Gamma-ray: bursts

1 INTRODUCTION

Gamma Ray Bursts (GRBs) have extremely high energetics. The isotropic equivalent energy E_{iso} , released during the prompt phase, is distributed over four orders of magnitudes in the range 10^{50} – 10^{54} erg. E_{iso} correlates with E_p , i.e. the peak of the νF_ν spectrum (Amati et al. 2002, 2009): $E_p \propto E_{\text{iso}}^{0.5}$. This holds for long duration GRBs. A similar correlation exists between the isotropic equivalent luminosity L_{iso} and E_p (Yonetoku et al. 2004) obeyed also by short events (Ghirlanda et al. 2009). The scatter of the data points around the $E_p - E_{\text{iso}}$ correlation, modeled with a Gaussian, has a dispersion $\sigma_{\text{sc}} = 0.23$ dex (see e.g. Nava et al. 2012 for a recent update of these correlations). This dispersion is much larger than the average statistical error $\bar{\sigma}_{E_{\text{iso}}} = 0.06$ dex and $\bar{\sigma}_{E_{\text{peak}}} = 0.10$ dex associated with E_{iso} and E_p , respectively.

Since E_{iso} is computed assuming that GRBs emit isotropically, it is only a proxy of the real GRB energetic. GRBs are thought

to emit their radiation within a jet of opening angle θ_{jet} . If the jet opening angle θ_{jet} is known, the *true energy* $E_\gamma \simeq E_{\text{iso}}\theta_{\text{jet}}^2$ and the *true GRB rate* can be estimated (Frail et al. 2001).

The estimate of θ_{jet} is made possible by the measure of the jet break time t_{break} , typically observed between 0.1 to >10 days in the afterglow optical light curve. Although θ_{jet} has been measured only for ~ 30 GRBs (Ghirlanda et al. 2007) it shows that:

(i) E_γ clusters around 10^{50} erg with a small dispersion (Frail et al. 2001; but see Racusin et al. 2009; Kocevski & Butler 2008);

(ii) E_γ is tightly correlated with E_p (Ghirlanda, Ghisellini & Lazzati 2004; Ghirlanda et al. 2007) with a scatter $\sigma_{\text{sc}} = 0.07$ dex (consistent with the average statistical error $\bar{\sigma}_{E_\gamma} = \bar{\sigma}_{E_p} \simeq 0.1$ dex associated with E_γ and E_p);

(iii) the true rate of local GRBs ranges from ~ 250 Gpc⁻³ yr⁻¹ (e.g. Frail et al. 2001) to ~ 33 Gpc⁻³ yr⁻¹ (Guetta, Piran & Waxman 2005). These different values are mainly due to the different values assumed for the collimation factor $f \propto \theta_{\text{jet}}^{-2}$. The true GRB rate can be compared with the local rate of SN Ib/c (e.g. Soderberg 2006; Guetta & Della Valle 2007; Grieco et al. 2012), i.e. the can-

* E-mail: giancarlo.ghirlanda@brera.inaf.it

didate progenitors of long GRBs, and allows to estimate the rate of orphan afterglows (e.g. Guetta et al. 2005).

The $E_p - E_{\text{iso}}$, $E_p - L_{\text{iso}}$ and $E_p - E_\gamma$ correlations could enclose some underlying feature of the GRB emission mechanism (e.g. Rees & Meszaros 2005; Ryde et al. 2006; Thompson 2006; Giannios & Spruit 2007; Thompson, Meszaros & Rees 2007; Panaitescu 2009), of the GRB jet structure (e.g. Yamazaki, Ioka & Nakamura 2004; Eichler & Levinson 2005; Lamb, Donaghy & Graziani 2005; Levinson & Eichler 2005) or of the progenitor (e.g. Lazzati, Morsony & Begelman 2011). An intriguing application of these correlations is the use of GRBs as standard candles (Ghirlanda, Ghisellini & Firmani 2005; Firmani et al. 2005; Amati et al. 2009).

The presence of outliers of the $E_p - E_{\text{iso}}$ correlation in the *CGRO/BATSE* GRB population (Band & Preece 2005; Nakar & Piran 2005; Shahmoradi & Nemiroff 2011) and in the *Fermi*/GBM burst sample (Collazzi et al. 2012) and the presence of possible instrumental biases (Butler et al. 2007; Butler, Kocevski & Bloom 2009; Kocevski 2012) caution about the use of these correlations either for deepening into the physics of GRBs and for cosmological purposes. Although instrumental selection effects are present, it seems that they cannot produce the correlations we see (Ghirlanda et al. 2008; Nava et al. 2008; Ghirlanda et al. 2012b). Moreover, a correlation between E_p and L_{iso} is present within individual GRBs as a function of time (Firmani et al. 2009; Ghirlanda et al. 2010; 2011; 2011a), suggesting that the radiative process(es) might be the origin of the $E_p - L_{\text{iso}}$ correlation. Despite these studies, the spectral energy correlations of GRBs and their possible applications are still a matter of intense debate.

A new piece of information recently added to the puzzle is that the GRB energetics (E'_{iso} , L'_{iso} and E'_p) appear nearly similar in the comoving frame (Ghirlanda et al. 2012 – G12 hereafter). To measure these comoving quantities¹ we have to know the bulk Lorentz factor Γ_0 , that can be estimated through the measurement of the peak time t_{peak} of the afterglow light curve. G12 could estimate Γ_0 in 30 long GRBs with known z and well defined energetics, finding that:

- (i) $E_{\text{iso}}(L_{\text{iso}}) \propto \Gamma_0^2$ and $E_p \propto \Gamma_0$;
- (ii) the comoving frame $E'_{\text{iso}} \sim 3.5 \times 10^{51}$ erg (dispersion 0.45 dex), $L'_{\text{iso}} \sim 5 \times 10^{48}$ erg s⁻¹ (dispersion 0.23 dex) and $E'_p \sim 6$ keV (dispersion 0.27 dex).

These results imply that the $E_p - E_{\text{iso}}$ and $E_p - L_{\text{iso}}$ correlation are a sequence of different Γ_0 factors (see also Dado, Dar & De Rujula 2007).

The θ_{jet} values of GRBs are known only for a couple of dozens of bursts (Ghirlanda et al. 2007). θ_{jet} appears distributed as a log-normal with a typical $\theta_{\text{jet}} \sim 3^\circ$ (Ghirlanda et al. 2005). By correcting the isotropic comoving frame energy E'_{iso} by this typical jet opening angle, the comoving frame true energy E'_γ results $\sim 5 \times 10^{48}$ erg. In G12 we also argued that in order to have consistency between the $E_p - E_\gamma$ and the $E_p - E_{\text{iso}}$ correlations one must require $\theta_{\text{jet}}^2 \Gamma_0 = \text{constant}$. A possible anti-correlation between θ_{jet} and Γ_0 is predicted by models of magnetically accelerated jets (Tchekhovskoy, McKinney & Narayan 2009; Komissarov, Vlahakis & Koenigl 2010) but, at present, only 4 GRBs have an estimate of θ_{jet} and Γ_0 and well constrained spectral properties.

The measure of θ_{jet} relies on the measure of t_{break} , that in turn requires the follow up of the optical afterglow emission up to

a few days after the burst explosion (Ghirlanda et al. 2007). The measurement of t_{break} is difficult, not only because it requires a large investment of telescope time, but also because several t_{break} are chromatic (contrary to what predicted; but see Ghisellini et al. 2009), and the jet break can be a smooth transition whose measurement requires an excellent sampling of the afterglow light curve (e.g. Van Eerten et al. 2010, 2011). Another complication is that the early afterglow emission is characterized by several breaks. For instance, the end of the plateau phase typically observed in the X-ray light curves, if misinterpreted as a jet break, biases the θ_{jet} distribution towards small values of θ_{jet} (Nava, Ghisellini & Ghirlanda 2006). Finally, the measure of large θ_{jet} is complicated by the faintness of the afterglow and its possible contamination by the host galaxy emission and the supernova associated to the burst. Several observational biases could shape the observed θ_{jet} distribution. Among these the fact that more luminous bursts (i.e. those more easily detected) should have the smallest jet opening angles. For all these reasons the *observed* distribution of θ_{jet} might not be representative of the real distribution of GRBs jet opening angles.

The distribution of Γ_0 is centered around $\Gamma_0=65$ (130) in the case of a wind (uniform) density distribution of the circum-burst medium. The distribution of Γ_0 is broad and extends between $\Gamma_0 \sim 20$ and $\Gamma_0 \sim 800$. These results are still based on a sample of only 30 GRBs (G12). The difficulties of early follow-up of the optical afterglow emission could prevent the measure of very large Γ_0 on the one hand, while the possible contamination by flares (Burrows et al. 2005; Falcone et al. 2007) or by other (non afterglow) emission components (e.g. Ghisellini et al. 2010) at intermediate times could prevent the estimate of the low-end of the Γ_0 distribution. One could argue if GRBs can have Γ_0 of a few. While there are some hints that GRB060218 should have $\Gamma_0 \sim 5$ (Ghisellini et al. 2006) the classical compactness argument, for typical GRB parameters (e.g. Piran 1999), requires that $\Gamma_0 \geq 100-200$. This argument was successfully applied to few bursts observed up to GeV energies by LAT on board Fermi (e.g. Abdo et al. 2009, Ghirlanda et al. 2009) to derive lower limits of several hundreds on Γ_0 . If, instead, the highest energy photon detected has an energy of say $E_{\text{max}} \sim 3$ MeV, the lower limit derived from the classical compactness argument would be $\Gamma_0 > \text{a few}$ (i.e. $\sim 2E_{\text{max}}/m_e c^2$). Therefore, also in the case of Γ_0 , the *observed* distribution, derived with still few events, could be not representative of the real distribution of this parameter.

The main aim of this paper is to constrain the distribution of Γ_0 and θ_{jet} in GRBs using the available independent constraints. This aim can be translated into a simple question: do θ_{jet} and Γ_0 follow power law distributions or do they follow some kind of peaked distribution (e.g. a broken power law or a log-normal)? In both cases the resulting distributions could be different from the observed ones since some selection effect (as discussed above) might prevent to measure very low and/or high values of Γ_0 and θ_{jet} . Another scope of the present paper is to test which is (if any) the relation between θ_{jet} and Γ_0 . A relation $\theta_{\text{jet}}^2 \Gamma_0 = \text{const}$ was assumed in G12 to explain the spectral energy correlations and a similar relation seems to arise from numerical simulations of jet accelerations (Tchekhovskoy et al. 2012). Here we use several observational constraints and test whether there is a $\theta_{\text{jet}}^a \Gamma_0 = \text{const}$ relation and try to constrain its exponent a . One important effect that we consider in this paper for the first time is the collimation of the burst radiation when Γ_0 is small. In general we are led to think that given a value of the collimation corrected energy E_γ , the corresponding isotropic equivalent energy is $E_{\text{iso}} \sim E_\gamma / \theta_{\text{jet}}^2$. This is true if the beaming of the radiation is “dominated” by the jet opening an-

¹ Primed quantities are in the comoving frame of the source.

gle, i.e. $1/\Gamma_0 \leq \sin\theta_{\text{jet}}$. However, GRBs with very low Γ_0 could have $1/\Gamma_0 \geq \sin\theta_{\text{jet}}$ and in this case the isotropic equivalent energy is determined by Γ_0 (i.e. $E_{\text{iso}} \sim E_\gamma \Gamma_0^2$ - see §. 2.2) rather than by θ_{jet} . This effect, introduces a limit ($\propto E_{\text{iso}}^{1/3}$) in the classical $E_p - E_{\text{iso}}$ plane (Fig.1) accounting for the absence of bursts with intermediate/low E_p and large values of E_{iso} . This limit can also partly account for the problem of ‘‘missing jet breaks’’ since these bursts with $1/\Gamma_0 \geq \sin\theta_{\text{jet}}$ should not show any jet break in their afterglow light curve (§4.5).

We rely on a GRB population synthesis code that we have recently adopted to explore the issue of instrumental selection biases on the $E_p - L_{\text{iso}}$ correlation (Ghirlanda et al. 2012b).

The simulation steps are described in §2 while the observational constraints that we aim to reproduce are outlined in §3. In §4 we present our results. We summarize and discuss our findings in §5. Throughout the paper a standard flat universe with $h = \Omega_\Lambda = 0.7$ is assumed.

2 POPULATION SYNTHESIS CODE

So far, the approach adopted in studying the spectral–energy correlations and the distributions of θ_{jet} or Γ_0 was (i) to derive the collimation corrected $E_p - E_\gamma$ correlation by correcting the isotropic energy E_{iso} for the collimation factor $\propto \theta_{\text{jet}}^2$ (e.g. Ghirlanda et al. 2004), or (ii) to derive the comoving frame properties of GRBs by correcting, for the Γ_0 factor, the isotropic values E_{iso} , L_{iso} and E_p (G12).

In this paper, we tackle the problem from the opposite side and jointly work with θ_{jet} and Γ_0 : we assume that GRBs have all the same comoving frame E'_p and E'_γ , and simulate GRB samples with different distributions of Γ_0 and θ_{jet} . This produces a population of GRBs with known energetics E_{iso} , peak energy E_p and observer frame fluence F and peak flux P . We would like to stress that our main assumption (same E'_p and E'_γ for all burst) is a crude simplification. Nevertheless, our assumption can work if the real E'_p and E'_γ distributions are indeed narrower than the distributions of the corresponding observed quantities. Recently, Giannios 2012 have shown that in photospheric models a comoving frame peak energy $E'_p \sim 1.5$ keV is expected.

The observational constraints that we aim to reproduce (see §3) are: (i) the rate of GRBs observed by *Swift*/BAT, *CGRO*/BATSE and *Fermi*/GBM, (ii) the $E_p - E_{\text{iso}}$ correlation defined by the complete sample of *Swift* bright bursts (Salvaterra et al. 2012; Nava et al. 2012) and (iii) the fluence and peak flux distributions of the population of bursts detected by *Fermi*/GBM (Goldstein et al. 2012) and *CGRO*/BATSE (Meegan et al. 1998).

Note that, since one of the aims of the present paper is to constrain the distributions of θ_{jet} and Γ_0 we cannot adopt the observed ones (discussed in the introduction) as constraints, otherwise we would fall into a circular argument. The distributions of Γ_0 and θ_{jet} that we assume in our simulations (power law, broken power law, log–normal) have all their characteristic parameters (slope, normalization, break values, width etc.) free to vary. These parameters are what we aim to constrain through our population synthesis code.

In Fig. 1 we show the rest frame peak energy E_p versus the total energy E (where E here is generically used to indicate an energy, either isotropic or collimation corrected). We highlight different regions (I, II and III) that are useful to explain the simulation steps (§2.1). This plane will be one of our observational constraints: in Fig. 1 we show (black filled points) the *Swift* complete sample

of bursts (Salvaterra et al. 2012; Nava et al. 2012) which we aim to reproduce through our simulations.

2.1 Simulation steps

Our starting assumption is that all GRBs have the same comoving frame $E'_p = 1.5$ keV and $E'_\gamma = 1.5 \times 10^{48}$ erg. This is shown by the black circle in Fig. 1. G12 find that $L'_{\text{iso}} \sim \text{const}$ and that the observed duration T_{90} does not depend on Γ_0 . Therefore, in the comoving frame, $T'_{90} \propto \Gamma_0 T_{90} \propto \Gamma_0$. It follows that $E'_\gamma = L'_{\text{iso}} T'_{90} \theta_{\text{jet}}^2$ is also constant if, as discussed in G12, $\theta_{\text{jet}}^2 \Gamma_0 = \text{const}$. Although some dispersion of the values of E'_p is present in the sample of G12, the value of E'_p that we assume here is consistent at the 2σ level of confidence with the distribution of values reported in G12 for the wind density ISM.

The main steps of our simulation are:

(i) we simulate a population of GRBs distributed in redshift z between $z = 0$ and $z = 10$ according to the GRB formation rate (GRBFR) $\psi(z)$. This is formed by two parts: $\psi(z) = e(z)R(z)$. The first term is a cosmic evolution term, while $R(z)$ is taken from Li (2008) (which extended to higher redshifts the results of Hopkins & Beacom 2008):

$$R(z) = \frac{0.0157 + 0.118z}{1 + (z/3.23)^{4.66}} \quad (1)$$

$R(z)$ is in units of $M_\odot \text{ yr}^{-1} \text{ Mpc}^{-3}$. Concerning $e(z)$, Salvaterra et al. (2012) derived the luminosity function of GRBs by jointly fitting the redshift distribution of a complete sample of bright GRBs detected by *Swift* and the count distribution of a larger sample of BATSE bursts. They found that either the evolution of the luminosity function or the evolution of the density of GRBs is required in order to account for these data sets. We assume the same term $e(z) = (1 + z)^{1.7}$ found by S12.

(ii) We assign to each GRB a bulk Lorentz factor Γ_0 extracted from a specified distribution, in the range $[1, 8000]$. The upper limit ($\Gamma_{0,\text{max}} = 8000$) is somewhat arbitrary, but large enough to encompass all the values of Γ_0 estimated so far, and in particular the large values derived for the few GRBs detected by the LAT instrument on board *Fermi*, if the GeV emission is interpreted as afterglow (Ghisellini et al. 2010).

For each simulated burst the rest frame peak energy E_p and the energy E_γ are (see G12):

$$E_{\text{peak}} = E'_{\text{peak}} \frac{5\Gamma_0}{5 - 2\beta_0}; \quad E_\gamma = E'_\gamma \Gamma_0 \quad (2)$$

where $\Gamma_0 = 1/(1 - \beta_0^2)^{1/2}$. The simulated bursts define a correlation between E_p and E_γ :

$$E_{\text{peak}} = \frac{E'_{\text{peak}}}{E'_\gamma} \frac{5E_\gamma}{5 - 2\beta_0} \propto \frac{E_\gamma}{5 - 2\beta_0} \quad (3)$$

for $\beta_0 \sim 1$ this corresponds to the $E_p - E_\gamma$ correlation in the case of a wind density profile (Nava et al. 2006). This relation is shown in Fig. 1 with the solid black line (labelled $E_p \propto E_\gamma$). The simulated Γ_0 distribute E_p between 1.5 keV ($\Gamma_0=1$) and ~ 20 MeV ($\Gamma_0=8000$).

(iii) We assign to each simulated burst a jet opening angle $\theta_{\text{jet}} \in [1^\circ, 90^\circ]$ extracted from a specified distribution.

(iv) The probability for a burst to be observed from the Earth depends on the viewing angle θ_{view} between the jet axis and the line of sight of the observer. We extract randomly a viewing angle θ_{view} from the cumulative distribution of the probability density function $\sin\theta_{\text{view}}$.

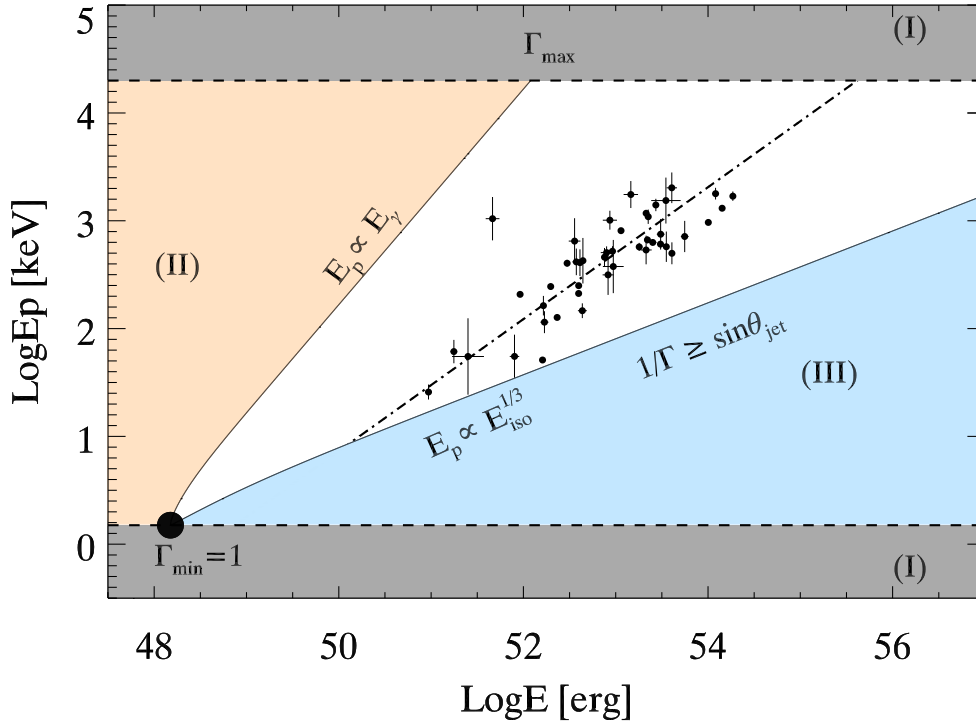


Figure 1. Rest frame plane of GRB energetics. The large black dot corresponds to the main assumption of our simulations, i.e. that all bursts have similar comoving frame $E'_p=1.5$ keV and $E'_\gamma=1.5\times 10^{48}$ erg. Assigning a certain Γ_0 to the burst, this moves along the line $E_p \propto E_\gamma$. Since $\Gamma_0 > 1$ and we assume a maximum Γ_0 of 8000, regions (I) are forbidden. Since all our simulated bursts have $\theta_{\text{jet}} \leq 90^\circ$, they cannot lie in region (II). When Γ_0 is small, the beaming cone $\sim 1/\Gamma_0$ can become wider than the aperture of the jet. In this case the isotropic equivalent energy becomes $E_{\text{iso}}=E_\gamma(1+\beta_0)\Gamma_0^2$, that is smaller than the energy calculated through $E_{\text{iso}}=E_\gamma/(1-\cos\theta_{\text{jet}})$. This introduces a limit $E_p \propto E_{\text{iso}}^{1/3}$ and bursts cannot lie on the right of this limit. Consequently, region (III) is forbidden. The black dots correspond to the real GRBs of the *Swift* complete sample. The fit to the *Swift* complete sample is shown by the dot-dashed line.

(v) In order to compare the simulated bursts with the source count distribution of existing samples of GRBs (see §3) we compute the observer frame peak fluxes P and fluences F . To this aim we assume a typical spectrum described by the Band function (Band et al. 1993), with low and high photon spectral indexes $\alpha = -1.0$ and $\beta = -2.3$, respectively (i.e. corresponding to the typical values observed by different instruments – e.g. Kaneko et al. 2006; Sakamoto et al. 2011)². The fluence F of each simulated burst in a given energy range is computed by re-normalizing this spectrum through the bolometric fluence $F_{\text{bol}}=E_{\text{iso}}(1+z)/4\pi d_L^2$, where d_L^2 is the luminosity distance for a given redshift z . To derive the peak flux P , we assign to each burst an (observer frame) duration T_{90} extracted from a distribution centered at 27.5 s and with a dispersion $\sigma_{\text{Log}T_{90}} = 0.35$. This distribution is truncated at $T_{90} = 2$ s because we consider only long duration GRBs in this analysis. Such a duration distribution is similar to that of the *Fermi*/GBM GRBs (Paciesas et al. 2012; Goldstein et al. 2012) and includes also very long bursts with $T_{90} \sim 300$ s. We assume that the bursts have a simple triangular light curve and derive the peak luminosity as $L_{\text{peak}} = 2E_{\text{iso}}(1+z)/T_{90}$. The peak flux P in a given energy range is obtained by re-normalizing the spectrum through the bolometric peak flux $P_{\text{bol}} = L_{\text{peak}}/4\pi d_L^2$.

2.2 Computation of E_{iso}

The isotropic equivalent energy E_{iso} of the simulated bursts can be derived from E_γ . Since $\theta_{\text{jet}} \leq 90^\circ$, simulated bursts cannot be in region II of Fig. 1 and E_{iso} can take values on the right hand side of the limit of Eq. 3 shown in Fig. 1. According to the values of θ_{jet} and Γ_0 assigned to each simulated bursts, the isotropic equivalent energy is:

$$E_{\text{iso}} = E_\gamma / (1 - \cos \theta_{\text{jet}}) \quad \text{if} \quad 1/\Gamma_0 \leq \sin \theta_{\text{jet}} \quad (4)$$

$$E_{\text{iso}} = E_\gamma (1 + \beta_0) \Gamma_0^2 \quad \text{if} \quad 1/\Gamma_0 > \sin \theta_{\text{jet}} \quad (5)$$

In the latter case E_{iso} is smaller than in Eq. 4. This introduces a limit in the $E_p - E_{\text{iso}}$ plane of Fig. 1 corresponding to the line:

$$E_{\text{peak}} \propto \left[\frac{E_{\text{iso}}}{(5 - 2\beta_0)^3 (1 + \beta_0)} \right]^{1/3} \quad (6)$$

(labelled $E_p \propto E_{\text{iso}}^{1/3}$ in Fig. 1). For a given θ_{jet} , bursts with a small value of Γ_0 will have an E_{iso} computed through Eq. 5 and will lie on the limiting line of region III in Fig. 1. Their radiation is, indeed, collimated within an angle $\arcsin(1/\Gamma_0)$ which is larger than their θ_{jet} .

Simulated bursts can populate the region delimited by boundaries (I, II and III) in Fig. 1. This is one (among others) observational constraint that we will adopt in our simulations (§3) to con-

² These values are also assumed by S12 to constrain the LF of GRBs.

strain the distributions of Γ_0 and θ_{jet} and their possible relation. According to the relative values of θ_{jet} , Γ_0 and θ_{view} , simulated bursts are classified as: bursts ‘‘pointing to us’’ (PO, hereafter), i.e. those that can be seen from the Earth, with $\sin\theta_{\text{view}} \leq \max[\sin\theta_{\text{jet}}, 1/\Gamma_0]$ and bursts pointing in other directions (NPO, hereafter), i.e. not observable from the Earth, with $\sin\theta_{\text{view}} > \max[\sin\theta_{\text{jet}}, 1/\Gamma_0]$. We will compare the PO simulated bursts with our observational constraints, while the entire population of simulated bursts (i.e. PO and NPO) will be used to infer the properties of GRBs (e.g. the distributions of Γ_0 and θ_{jet} and the true burst rate).

3 OBSERVATIONAL CONSTRAINTS

In order to test whether θ_{jet} and Γ_0 assume characteristic values or not we compare the population of simulated bursts with real samples of GRBs. In this section we describe our observational constraints. We consider the ensemble of GRBs detected by the Burst Alert Telescope (BAT) on board *Swift*, the Gamma Burst Monitor (GBM) on board *Fermi* and the Burst And Transient Source Experiment (BATSE) on board the *Compton Gamma Ray Observatory* (CGRO).

3.1 The *Swift* BAT complete sample

Salvaterra et al. (2012 - S12 hereafter) constructed a sample of bright *Swift* bursts consisting of 58 GRBs detected by *Swift*/BAT with $P \geq P_{\text{lim}} = 2.6 \text{ ph cm}^{-2} \text{ s}^{-1}$ (integrated in the 15–150 keV energy range). Fifty four of these events have a measured redshift z so that the S12 sample is 90% complete in redshift. Forty six (out of 54) GRBs in this sample have well determined spectral properties (filled circles in Fig. 1) and define a statistically robust $E_p - E_{\text{iso}}$ correlation with rank correlation coefficient $\rho = 0.76$ and chance probability $P = 7 \times 10^{-10}$ (Nava et al. 2012, N12 hereafter)³. The correlation properties (slope and normalization) of the complete *Swift* sample are consistent with those defined with the incomplete larger sample of 136 bursts with known z and spectral parameters (see N12). Therefore, the distribution of the *Swift* complete sample (46/54 events with well constrained E_p) in the $E_p - E_{\text{iso}}$ plane is representative of the larger (heterogeneous) population of GRBs with measured z and well constrained spectral properties. The 46 GRBs of the complete *Swift* sample define a correlation $E_p \propto E_{\text{iso}}^{0.61 \pm 0.06}$ (shown by the dot-dashed line in Fig. 1) with a scatter (computed perpendicular to the best fit line) with a Gaussian dispersion $\sigma = 0.29$ dex.

The *Swift* complete sample of S12 contains $\sim 1/3$ of the bursts detected by *Swift*⁴ with $P \geq 2.6 \text{ ph cm}^{-2} \text{ s}^{-1}$. We verified that the *Swift* complete sample of 54 events selected by S12 is representative of the larger population of 149 long *Swift* bursts with $P \geq P_{\text{lim}}$: the Kolmogorov–Smirnov test on the peak flux distribution of the two samples gives a probability of 0.6 that the two distributions are drawn from the same parent population. These bursts were not included in the selection of S12 because they do not have favorable conditions for ground-based follow up.

These 149 events with $P \geq P_{\text{lim}}$ are the bursts detected by *Swift* in ~ 7 yrs from its launch within the (half coded) field of view

³ The 8 GRBs without a secure estimate of the redshift or with incomplete spectral informations are consistent with the $E_p - E_{\text{iso}}$ correlation defined by the 46 GRBs discussed here, see N12 for details.

⁴ http://swift.gsfc.nasa.gov/docs/swift/archive/grb_table/

of ~ 1.4 sr of BAT. This corresponds to an average *Swift* detection rate of $\mathcal{R}_{\text{Swift}} \sim 15 \text{ events sr}^{-1} \text{ yr}^{-1}$.

3.2 The *Fermi* GBM sample

Another observational constraint that we consider is the population of bursts detected by the GBM on board *Fermi*. The spectral properties of GBM bursts have been studied in Nava et al. (2011a) and compared to those of BATSE bursts in Nava et al. (2011b). More recently, the first release of the GBM spectral catalog (Goldstein et al. 2012) provided the spectral parameters and derived quantities (i.e. peak fluxes and fluences) for 487 GRBs detected by the GBM in its first 2 years of activity. 398 bursts in this catalog are long events and have measured peak flux P and fluence F (both integrated in the 10 keV–1 MeV energy range)⁵.

We cut the GBM sample to $P \geq P_{\text{lim}} = 2.5 \text{ ph cm}^{-2} \text{ s}^{-1}$, in order to account for the possible incompleteness of the sample at lower fluxes, obtaining 312 GBM bursts.

The GBM is an all sky monitor that observes on average ~ 60 – 70% of the sky. Therefore, the average GBM detection rate is $\mathcal{R}_{\text{GBM}} \sim 21 \text{ events sr}^{-1} \text{ yr}^{-1}$ with peak flux, integrated in the 10 keV–1 MeV energy range, $P \geq 2.5 \text{ ph cm}^{-2} \text{ s}^{-1}$.

3.3 The CGRO BATSE sample

We also consider the sample of GRBs detected by BATSE. The 4B sample (Meegan et al. 1998) contains 1540 long events and 1496 of these have their P and F (both integrated in the 50–300 keV energy range) measured. The sample of 1496 BATSE bursts is cut at $P \geq P_{\text{lim}} = 1 \text{ ph cm}^{-2} \text{ s}^{-1}$ with 716 BATSE bursts above this threshold. Considering the average portion of the sky observed by BATSE, i.e. $\sim 70\%$ of the sky, the detection rate of BATSE is $\mathcal{R}_{\text{BATSE}} \sim 16 \text{ events sr}^{-1} \text{ yr}^{-1}$ for GRBs with a peak flux, integrated in the 50–300 keV energy range, $P \geq 1 \text{ ph cm}^{-2} \text{ s}^{-1}$.

The lower detection rate of BATSE with respect to GBM is due to the different energy range where the peak fluxes are calculated (i.e. 10 keV–1 MeV for GBM and 50–300 keV for BATSE, respectively). We verified that by considering the GBM bursts with peak flux P integrated in the same energy range of BATSE (i.e. 50–300 keV) larger than $1 \text{ ph cm}^{-2} \text{ s}^{-1}$ (i.e. the same threshold adopted for BATSE), the GBM rate is equal to the BATSE one.

3.4 Extraction of results

From each simulation we extract three populations of GRBs among the bursts pointing to us (PO):

(i) the *Swift* comparison sample: *simulated* GRBs with peak flux, integrated in the 15–150 keV band, larger than $2.6 \text{ ph cm}^{-2} \text{ s}^{-1}$. We also require that their observer frame peak energy is in the range 15 keV–2 MeV. Indeed, this is the energy range where E_p^{obs} can be measured by presently flying satellites like *Swift*, Konus and *Fermi*.

(ii) the GBM comparison sample: *simulated* bursts with a peak flux, integrated in the 10 keV–1 MeV energy range, larger than $2.5 \text{ ph cm}^{-2} \text{ s}^{-1}$;

⁵ P and F are reported in Goldstein et al. (2012) and were obtained by integrating the model that best fits the peak time resolved spectrum and the time averaged spectrum, respectively.

(iii) the BATSE comparison sample: *simulated* bursts with a peak flux, integrated in the 50–300 keV energy range, larger than $1.0 \text{ ph cm}^{-2} \text{ s}^{-1}$.

The simulation is adjusted so that the *Swift* comparison sample contains 149 GRBs, i.e. the same number of bright bursts detected by *Swift* (§3.1). Therefore, the *Swift* rate $\mathcal{R}_{\text{Swift}}$ is imposed. What we derive instead from the simulation is the rate of GBM and BATSE GRBs that we compare with the real rates of these two instruments described in §3.2 and §3.3 respectively.

We also require that the *Swift* comparison sample is consistent with the *Swift* complete sample of S12. To this aim we compare them in the rest frame $E_p - E_{\text{iso}}$ plane and in the observer frame $E_{\text{peak}}^{\text{obs}} - F$ plane deriving a 2 dimensional Kolmogorov–Smirnov (KS) probability (one for the $E_p - E_{\text{iso}}$ and one for $E_{\text{peak}}^{\text{obs}} - F$ plane). We also verify through a 1 dimensional KS test that the redshift distribution of the *Swift* comparison sample is consistent with that of the *Swift* complete sample. Finally we compare, through a 1D–KS test, the fluence and peak flux distributions of the GBM and BATSE comparison samples with those of the real samples of GRBs detected by these instruments and described in §3.2 and §3.3, respectively.

Since the *Swift* complete sample contains only the brightest *Swift* bursts it maps the high P end of the peak flux distribution of GRBs. The GBM and BATSE samples that we adopt here extend the comparison sample to lower values of P and ensures that our simulations reproduce also the faint end of the GRB population⁶.

For each simulation we derive the following probabilities:

- the 2D-KS probability that the *Swift* comparison sample is consistent with the complete *Swift* sample of S12 in the $E_p - E_{\text{iso}}$ plane;
- the 2D-KS probability that the *Swift* comparison sample is consistent with the complete *Swift* sample of S12 in the $E_{\text{peak}}^{\text{obs}} - F$ plane;
- the 1D-KS probability that the *Swift* comparison sample has a redshift distribution consistent with that of the S12 *Swift* sample;
- the 1D-KS probabilities that the GBM comparison sample is consistent with the GBM sample in terms of peak flux P and fluence F ;
- the 1D-KS probabilities that the BATSE comparison sample is consistent with the BATSE sample in terms of peak flux P and fluence F ;
- we verify if the GBM rate predicted by the simulation is consistent, at 1σ , with the GBM rate \mathcal{R}_{GBM} .
- we verify if the BATSE rate predicted by the simulation is consistent, at 1σ , with the BATSE rate $\mathcal{R}_{\text{BATSE}}$.

For the KS probabilities we set a limit of 10^{-3} below which we consider that two distributions (either 1D or 2D) are inconsistent at more than 3σ . Each simulation, with its assumptions on the distribution of θ_{jet} and Γ_0 , is repeated 1000 times and we compute the percentage \mathcal{P} of repeated simulations that produce GRB samples (i.e. *Swift*, GBM and BATSE comparison samples) consistent with our observational constraints.

⁶ The P values of the GBM sample are computed on the broad 10 keV–1 MeV energy range (i.e. much broader than the 15–150 keV energy range of *Swift*). This ensures that the selected sample of the GBM bursts extends the population of GRBs to lower fluxes than those of the *Swift* complete sample.

4 RESULTS

In the following sections we present the results obtained with different possible assumptions for the distributions of Γ_0 and θ_{jet} . We want to test which one among the possible intrinsic distributions of Γ_0 and θ_{jet} that one can think of (e.g. power laws, broken power laws or log–normal) best reproduces the observational constraints described in the previous section.

4.1 Power law distributions of Γ_0 and θ_{jet}

We assume that both θ_{jet} and Γ_0 are distributed as power laws: $dN/d\theta_{\text{jet}} \propto \theta_{\text{jet}}^a$ and $dN/d\Gamma_0 \propto \Gamma_0^c$. This corresponds to the hypothesis that θ_{jet} and Γ_0 do not have a characteristic value. We consider $a \in [-2, -1]$ and $c \in [-2, -1]$.

The choice of these parameters corresponds to have most of the simulated bursts with low Γ_0 factors and with small θ_{jet} values. One could think that such distributions are already excluded by the observed distributions of θ_{jet} and Γ_0 (which are log–normal) discussed in §1. However, those are the *observed* distributions of Γ_0 and θ_{jet} and they are subject to several biases (see §1). The intrinsic distributions might well be completely different and this motivates to start with this simplest assumption, i.e. that both Γ_0 and θ_{jet} have power law distributions.

Under the hypothesis that both Γ_0 and θ_{jet} have power law distributions (with free parameters a and c varied in the above ranges with a step 0.2 in both parameters), only in 1% of 1000 repeated simulations we can find an agreement with all our observational constraints. In order to show the inconsistency of the simulations with the observational constraints we present in Fig. 2 the results of the simulations assuming that θ_{jet} and Γ_0 have power law distributions with $a = c = -1$. This case, shown as an example, corresponds to a uniform distribution of $\text{Log}\Gamma_0$ and $\text{Log}\theta_{\text{jet}}$.

The rest frame $E_p - E_{\text{iso}}$ plane (top left panel in Fig. 2) is filled uniformly with simulated bursts (yellow dots) distributed between the $E_p - E_\gamma$ limit and with a minimum $\theta_{\text{jet}}=1^\circ$ (the oblique right limit to the distribution of yellow dots). The simulated GRBs pointing to us (PO) have preferentially large θ_{jet} values (blue dots in the top left panel of Fig. 2). The simulated bursts of the *Swift* comparison sample (here represented by the smoothed density contours⁷ – red solid lines in Fig. 2) are inconsistent with the real GRBs of the *Swift* complete sample (open squares). The red contours extend at high E_p values where there is a deficit of *Swift* bursts and they also over predict the number of bursts on the right hand side of the distribution of the real *Swift* bursts (i.e towards large values of E_{iso} for intermediate/high values of E_p).

Also in the observer frame $E_{\text{peak}}^{\text{obs}} - F$ plane (top right panel in Fig. 2) the simulated *Swift* comparison sample (solid contours) are inconsistent with the real *Swift* bursts of the complete sample (open squares). Simulated bursts of the *Swift* comparison sample tend to concentrate towards the upper part of the $E_{\text{peak}}^{\text{obs}} - F$ plane.

The bottom panels of Fig. 2 show the cumulative rate distribution of the fluence for the GBM and BATSE sample (right and left panels of Fig. 2) compared with the predictions of the simulations (dashed regions in the bottom panels of Fig. 2). The rate of GBM and BATSE bursts predicted by the simulation which assumes a power law distribution for both θ_{jet} and Γ_0 (with index -1) is a factor ~ 2 larger than the rate of GBM bursts. Also the distributions

⁷ These are obtained by staking 1000 simulations and smoothing the obtained distribution in the $E_p - E_{\text{iso}}$ plane.

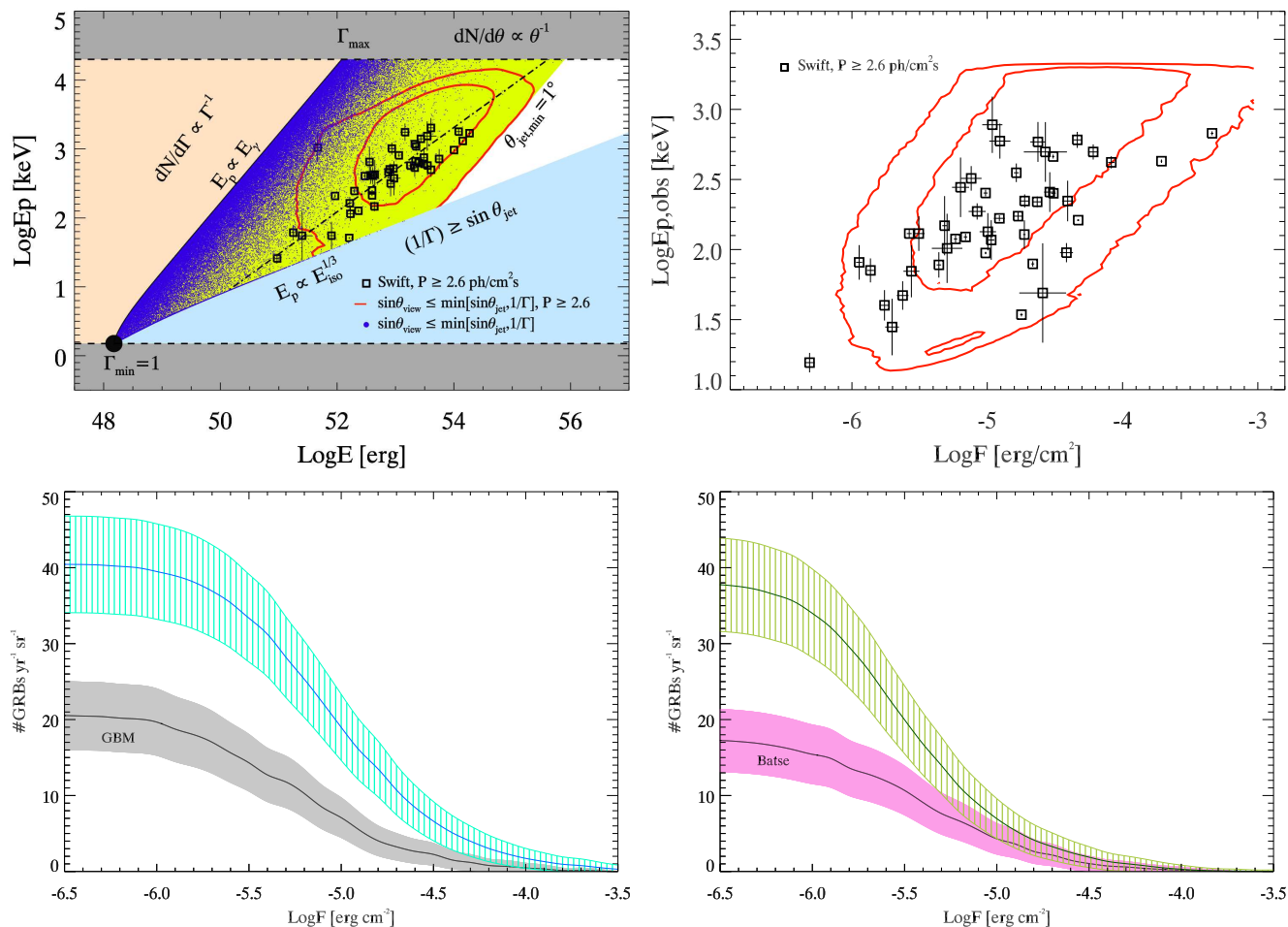


Figure 2. Result of the simulation assuming a power law distributions of θ_{jet} and Γ_0 . *Top left:* rest frame $E_p - E_{\text{iso}}$ plane (regions and labels as in Fig 1). The simulation assumes $a = c = -1.0$ (see §4.1) which correspond to uniform distributions in the logarithm of θ_{jet} and Γ_0 . The yellow dots represent all the simulated bursts, the blue dots show the PO bursts, i.e. those pointing to us. The red solid lines are the smoothed density contour (1 and 2 σ confidence levels) of the simulated *Swift* comparison sample. They should reproduce the distribution of the real *Swift* GRBs of the complete sample (open black squares). *Top right:* observer frame $E_{\text{peak}}^{\text{obs}} - F$ plane where the simulated *Swift* bursts (solid contours) are compared with the real GRBs of the *Swift* complete sample (open square symbols). *Bottom left:* cumulative rate distribution of GBM real bursts (solid black line) and its 1σ uncertainty (grey solid filled region) compared with the cumulative rate distribution of simulated GBM bursts (solid line and dashed cyan region corresponding to its 1σ uncertainty). *Bottom right:* cumulative rate distribution of BATSE real bursts (solid black line) and its 1σ uncertainty (pink filled solid region) compared with the prediction of the simulation (dashed region).

of the peak flux of the simulated BATSE and GBM samples are inconsistent with the real samples.

If we assume steeper power law distributions of θ_{jet} and Γ_0 [e.g. $(a, c) = (-2, -2)$], the excess of bursts with large peak energy (both in the rest frame and in the observer frame of Fig. 2, top left and right panels respectively) is reduced but the rate of simulated GBM and BATSE bursts increases becoming more inconsistent with the real rates of GRBs detected by these two instruments (bottom panels of Fig. 2). This result shows that all the constraints that we have adopted (§3) are relevant: the GBM and BATSE comparison sample map the low end of the peak flux/fluence distribution while the *Swift* complete sample maps the bright burst tail of such distributions. The bursts of the *Swift* complete sample, having their z measured, map the distribution of GRBs in the rest frame $E_p - E_{\text{iso}}$ plane.

4.2 Peaked distributions of Γ_0 and θ_{jet}

Since we could not find agreement between the simulations which assume power law distributions of θ_{jet} and Γ_0 and our observational constraints, we now consider the case of peaked distributions of θ_{jet} and Γ_0 .

The simplest assumption is that θ_{jet} and/or Γ_0 are distributed as broken power laws. We first assumed that only θ_{jet} or Γ_0 have a broken power law distribution, while the other parameter is distributed as a single power law. In this case we cannot find a percentage of repeated simulations larger than 2% in agreement with our observational constraints.

We then considered the case of a broken power law distribution for both θ_{jet} and Γ_0 :

$$\frac{dN}{d\theta_{\text{jet}}} = \begin{cases} \theta_{\text{jet}}^a & \text{if } \theta_{\text{jet}} \leq \theta_* \\ \theta_{\text{jet}}^b & \text{if } \theta_{\text{jet}} > \theta_* \end{cases}$$

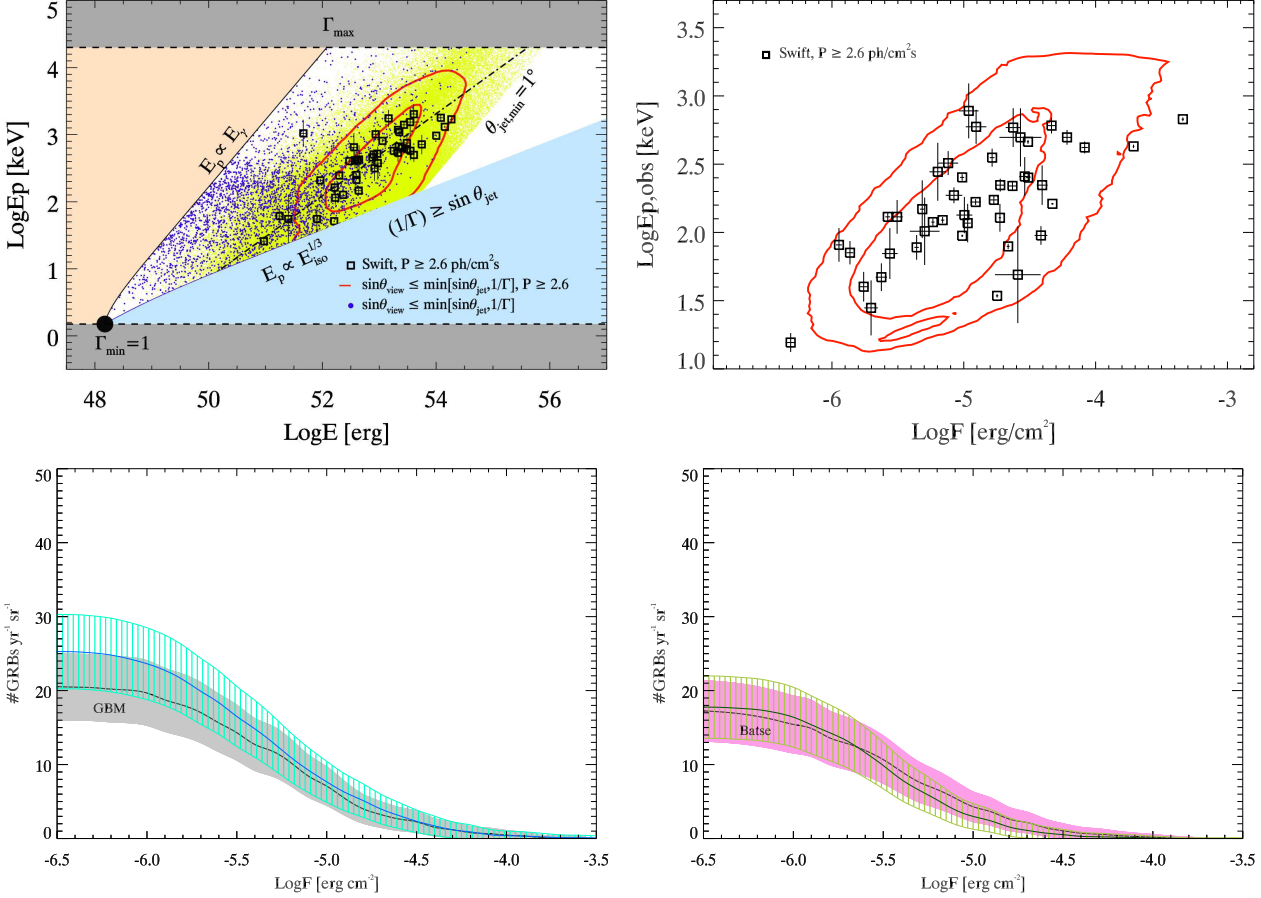


Figure 3. Result of the simulation assuming two broken power law distributions of θ_{jet} and Γ_0 (see text for the assumed values of the distribution parameters). Same plots and symbols as in Fig. 2.

$$\frac{dN}{d\Gamma_0} = \begin{cases} \Gamma_0^c & \text{if } \Gamma_0 \leq \Gamma_* \\ \Gamma_0^d & \text{if } \Gamma_0 > \Gamma_* \end{cases}$$

For the distribution of θ_{jet} we consider the following parameter ranges: $a \in [0.5, 2.0]$, $b \in [-2.0, -5.0]$ and $\theta_* \in [3^\circ, 12^\circ]$. For Γ_0 : $c \in [0.5, 2.0]$, $d \in [-2.0, -5.0]$ and $\Gamma_* \in [50, 120]$. The free parameters are varied with step 0.1 for a and b and 0.5° for θ_* for the broken power law distribution of θ_{jet} and with step 0.1 for c and d and 10 for Γ_* for the broken power law distribution of Γ_0 .

We find that at most $\sim 20\%$ of the 1000 repeated simulations reproduce our observational constraints when $(a, b, \theta_*) = (0.5, -3.0, 4.5^\circ)$ and $(c, d, \Gamma_*) = (1.8, -3.5, 70)$ with step 0.1 for c and d and 10 for Γ_* for the broken power law distribution of Γ_0 . A lower percentage of agreement is obtained for any other choice of the free parameters.

We show in Fig. 3 the results of the simulations with the above parameter values for the distributions of θ_{jet} and Γ_0 . We note that a better agreement is now found between the rate of the GBM and BATSE bursts (bottom panels of Fig. 3) while the distribution of simulated bursts of the *Swift* comparison sample (solid contours) are inconsistent with the *Swift* bursts of the complete sample both in the rest frame $E_p - E_{\text{iso}}$ plane (top left panel of Fig. 3) and in the observer frame plane $E_{\text{peak}}^{\text{obs}} - F$ (top right panel of Fig. 3).

The assumption of a characteristic value of Γ_0 corresponds to concentrate GRBs around a typical value of E_p (see Eq. 2). In this case the narrower θ_{jet} distribution reduces the number of simulated

bursts with large values of θ_{jet} , thus clustering the simulated GRBs of the PO class around the $E_p - E_\gamma$ limit of Fig. 3 (top left panel) that was found in the case of single power laws (§4.1).

A broken power law is a simple approximation of a peaked distribution. The real distribution of Γ_0 and θ_{jet} could have a different shape. We then considered the case of log-normal distributions for both Γ_0 and θ_{jet} , with central values of the θ_{jet} distribution between 3° and 12° (step 0.5°) and width between 0.3 and 0.8 (step 0.05) and central values of Γ_0 between 50 and 120 (step 5) and width between 0.2 and 0.8 (step 0.05). We find that, if θ_{jet} has a log-normal distribution with a median value of 4.5° (with a dispersion of 0.5) and Γ_0 is distributed as a log-normal with median 85 (with a dispersion of 0.45), the 40% of the 1000 repeated simulations is in agreement with all our observational constraints.

The latter assumption, that seems to improve the consistency between the simulated GRB population and the observational constraints, suggests that Γ_0 and θ_{jet} have log-normal distributions. However, the fact that no more than 40% of the repeated simulations can reproduce all our observational constraints, is suggesting that some ingredient is still missing. This is the subject of the next section where we study for the first time through our numerical simulations, the possibility that there is a relation between the average values of θ_{jet} and Γ_0 .

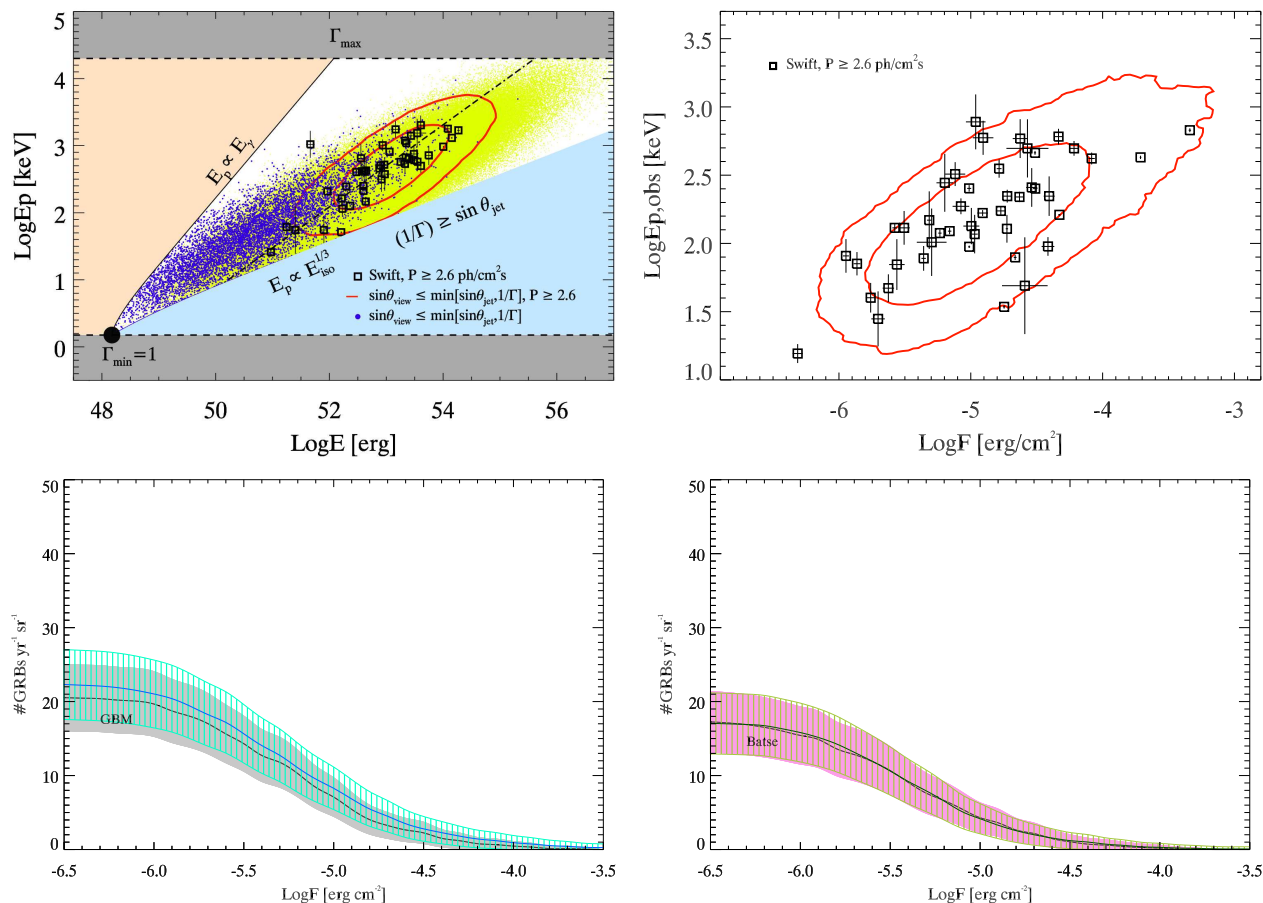


Figure 4. Simulations assuming log-normal distributions of θ_{jet} and Γ_0 and a relation between them (see text). Symbols and labels as in Fig. 2.

4.3 The relation between θ_{jet} and Γ_0

By assuming a θ_{jet} distribution with a characteristic value as in §4.2, the simulated bursts in the $E_p - E_{\text{iso}}$ plane cluster around a correlation which is linear in this plane (i.e. parallel to the $E_p - E_\gamma$ limit), while the $E_p - E_{\text{iso}}$ correlation defined by the *Swift* complete sample (and similarly by the larger, incomplete, sample of bursts with measured redshift – see N12) has a flatter slope, i.e. $E_p \propto E_{\text{iso}}^{0.6}$. In other words, for an infinitely narrow distribution of θ_{jet} , the simulated bursts (yellow dots in Fig. 3 top left panel) would produce a linear $E_p - E_{\text{iso}}$ correlation which is inconsistent with the observed $E_p - E_{\text{iso}}$ correlation. This suggests that, besides the fact that θ_{jet} and Γ_0 should have characteristic values (i.e. peaked distributions), they should also be correlated.

Indeed, G12 find that the comoving frame properties of GRBs (and in particular the fact that $E_p \propto \Gamma_0$ and $E_{\text{iso}} \propto \Gamma_0^2$) can be combined to explain both the $E_p \propto E_{\text{iso}}^{0.5}$ and the $E_p \propto E_\gamma$ correlation if the ansatz $\theta_{\text{jet}}^2 \Gamma_0 = \text{const}$ is valid. Several recent numerical simulations of jet acceleration in GRBs suggest that a link between Γ_0 and θ_{jet} should exist, although the form of this relation depends on several assumptions of these simulations. In this section we explore, for the first time, if a relation $\theta_{\text{jet}}^m \Gamma_0 = K$ can account for the observational constraints described in §3 and in this case we constrain its free parameters (m and K). We start from the result of the previous section, which showed that the best result (i.e. 40% of the repeated simulations are in agreement with the observations) is obtained assuming two log-normal distributions for Γ_0 and θ_{jet} .

We simulate bursts with $\text{Log}\Gamma_0$ distributed as a Gaussian with a characteristic central value $\text{Log}\Gamma_*$ and a dispersion $\sigma_{\text{Log}\Gamma_0}$. Similarly we assume a Gaussian distribution for $\text{Log}\theta_{\text{jet}}$ centered at $\text{Log}\theta_{*,\text{jet}}$ and with a dispersion $\sigma_{\text{Log}\theta_{\text{jet}}}$. We then assume that there is a relation between θ_{jet} and Γ_0 of the form $\text{Log}\theta_{*,\text{jet}} = -1/m \text{Log}\Gamma_* + q$. In this way the distribution of $\text{Log}\theta_{\text{jet}}$ is centered on a value which is given by the assumed relation between θ_{jet} and Γ_0 .

We explored the parameter space (defined by 5 free parameters) and found that 80% of our simulations are consistent with our constraints if $\text{Log}\Gamma_* = 1.95$ with a dispersion of $\sigma_{\text{Log}\Gamma_0} = 0.65$ dex, $m = 2.5$, $q = 1.45$ and $\sigma_{\text{Log}\theta_{\text{jet}}} = 0.3$ dex.

We show in Fig. 4 the results of this simulation which assumes log-normal distributions of Γ_0 and θ_{jet} and a relation between these two parameters. In the $E_p - E_{\text{iso}}$ plane (top left panel in Fig. 4) and in the $E_{p,\text{peak}}^{\text{obs}} - F$ plane (top right in Fig. 4) we find a good agreement between the simulated *Swift* comparison sample (solid contours) and the real *Swift* complete sample (open squares). Now the predicted rate of GBM and BATSE bursts is fully consistent with the real ones (bottom left and right panels in Fig. 4 respectively).

We stress that, given the assumptions of our simulation (e.g. the spectrum, duration and unique values of the comoving frame energetics of all GRBs) we do not expect to find 100% of the simulations reproducing our constraints. However, we can use our code to derive interesting properties of the population of GRBs. Indeed, in our simulations we generate a population of GRBs pointing in

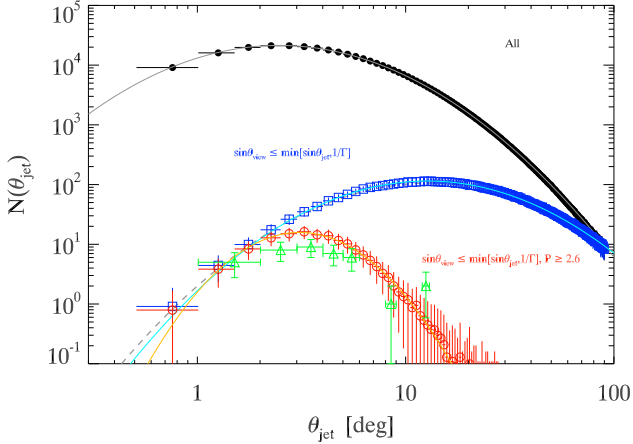


Figure 5. Distribution of θ_{jet} of GRBs. The θ_{jet} distribution of the total sample of simulated GRBs is shown by the filled circles. The solid grey line shows the fit with a lognormal function (Eq.7). The subsample of GRBs pointing towards the Earth (PO) is shown by the open (blue) squares and its fit with a lognormal by the cyan line. The sample of PO GRBs and peak flux $P \geq 2.6 \text{ cm}^{-2} \text{ s}^{-1}$ (i.e. the *Swift* comparison sample) is shown by the open (red) circles and its lognormal fit by the orange line. The dashed (grey) line shows the lognormal fit of the distribution of all the bursts (solid grey line) multiplied by $1 - \cos \theta_{\text{jet}}$. The green triangles show the distribution of the 27 GRBs with measured jet opening angle collected in Ghirlanda et al. (2004, 2007).

every direction. Only those pointing towards the Earth (PO) are then compared with existing samples of GRBs (like those described in §3). This is also the population of bursts that will be explored by future GRB detectors with better sensitivity than the present ones. We can derive the properties of the whole GRB population (i.e. all the bursts pointing in whatever direction), like the jet opening angle distribution, the bulk Lorentz factor distribution and the true GRB rate.

4.4 θ_{jet} distribution of GRBs

From the best simulation described in §4.3 we can derive the distribution of the jet opening angle of GRBs. In Fig. 5 we show the distribution of θ_{jet} for all the simulated bursts (black points) and for the PO bursts (open cyan squares). The population of GRBs pointing towards the Earth and with a peak flux $P \geq 2.6 \text{ cm}^{-2} \text{ s}^{-1}$ in the 15–150 keV range (i.e. the *Swift* comparison sample) is shown by the open (red) circles. All the distributions of θ_{jet} can be modeled with a log normal function:

$$N(x) = \frac{A}{x\sigma\sqrt{2\pi}} \exp \left[-\frac{(\ln x - \mu)^2}{2\sigma^2} \right] \quad (7)$$

where the free parameters are (μ, σ) and the normalization A . The best fit parameters μ and σ are reported in Tab. 1. The peak of the log-normal distribution, i.e. its mode, is $\exp(\mu - \sigma^2)$, the mean is $\exp(\mu + \sigma^2/2)$ and the median is $\exp(\mu)$. Since the asymmetry of the log-normal distributions can be considerably large, we report in Tab. 1 all these moments.

The θ_{jet} of GRBs of the *Swift* comparison sample (red open circles in Fig. 5) have a mean of $\theta_{\text{jet}} \sim 4.7^\circ$. This distribution is consistent with the θ_{jet} estimated from the break of the optical light curves (Ghirlanda et al. 2004, 2007), shown by the open (green) triangles in Fig. 5.

The GRBs that point to the Earth (PO - shown by the open blue squares in Fig. 5) have a θ_{jet} distribution peaking at considerably larger values (40° - see Tab.1) than the entire GRB population. This can be easily interpreted: consider the distribution of the entire population of GRBs (black dots in Fig. 5) which contains all bursts pointing in every direction. The probability that a burst with a certain θ_{jet} is pointing to us is proportional to $(1 - \cos \theta_{\text{jet}})$. Therefore the distribution of θ_{jet} for PO bursts is obtained from the total distribution by multiplying by $(1 - \cos \theta_{\text{jet}})$. This reduces the number of bursts per unit θ_{jet} and also shifts the peak of the PO distribution towards an average larger value. This is shown in Fig. 5 by the dashed (grey) line which is obtained by multiplying the fit of the distribution of θ_{jet} of the entire GRB population (solid grey line in Fig. 5) by $(1 - \cos \theta_{\text{jet}})$ and it fits the distribution of the PO bursts (open squares in Fig. 5).

Among the simulated bursts that are pointing towards the Earth we considered the bright bursts (i.e. selected with the same peak flux threshold of the *Swift* complete sample). These bursts tend to have small jet opening angles and this accounts for their θ_{jet} distribution peaking at $\sim 5^\circ$ in Fig. 5 (open red circles).

Although apparently there is a similarity between the θ_{jet} distribution of all bursts (i.e. pointing in every direction) and the θ_{jet} distribution of the PO bright bursts, they differ by a factor 2 (1.8) in their peak values (and dispersions) which are reported in Tab.1.

The three distributions shown in Fig. 5 allow us to make some further considerations. If we could measure θ_{jet} for all bursts pointing towards the Earth (PO in Tab. 1), we would obtain the open (blue) square distribution of Fig. 5 with a mean $\sim 40^\circ$. However, the real θ_{jet} distribution of the population of GRBs (i.e. all the simulated bursts - black filled circles distribution in Fig. 5) has a mean of $\sim 8.7^\circ$ and it is more consistent with the distribution of the simulated PO bursts with large peak fluxes (the *Swift* comparison sample). This suggests that the bursts distributed in the high part of the $E_p - E_{\text{iso}}$ correlation, where are the bursts of the complete *Swift* sample (filled black dots in Fig. 4 top left panel), properly sample the peak of the θ_{jet} distribution of the entire GRB population.

4.5 GRBs with no jet break

It has been shown in §3 that if a burst has a Γ_0 such that $\sin \theta_{\text{jet}} \leq 1/\Gamma_0$, its E_{iso} is determined by Γ_0 (Eq. 5) and not by θ_{jet} . This value is lower than that computed by θ_{jet} (Eq. 4). In these bursts, therefore, we should not observe a jet break in their light curve since the emitted radiation is initially collimated within an angle $\arcsin 1/\Gamma_0$ larger than θ_{jet} . Since Γ decreases during the afterglow phase due to the deceleration of the fireball by the interstellar medium, in these bursts the jet break, corresponding to the transition $1/\Gamma \sim \theta_{\text{jet}}$, will never happen.

The above argument contributes to explain the fact that bursts might not show an evident jet break in their afterglow light curve if $1/\Gamma_0 \geq \sin \theta_{\text{jet}}$. However, in these bursts we expect that the afterglow light curve is declining with a typical post-break decay index $\sim -p$ (where p is the shock-accelerated electron energy distribution index - e.g. Panaitescu & Kumar 2001). Other possible explanations for the lack of t_{break} measurements have been proposed. Numerical simulations (e.g. Van Eerten et al. 2010), for instance, suggest that the jet break transition can be very smooth (almost difficult to be distinguished from a single power law decay with available data sets) due to a combination of the jet dynamics before and after the jet break time (and additional complications can be induced by the viewing angle effects when the observer is not on-axis). Although a detailed discussion of the missing jet breaks

Distrib.	sample	σ	μ	Mode	Mean	Median
θ_{jet}	ALL	0.916 ± 0.001	1.742 ± 0.002	2.47°	8.68°	5.71°
	PO	0.874 ± 0.010	3.308 ± 0.013	12.73°	40.04°	27.33°
	PO*	0.610 ± 0.020	2.83 ± 0.029	11.68°	20.41°	16.95°
	PO <i>Swift</i>	0.527 ± 0.032	1.410 ± 0.043	3.10°	4.71°	4.10°
	PO* <i>Swift</i>	0.544 ± 0.298	1.043 ± 0.434	2.11°	3.29°	2.83°
Γ_0	ALL	1.475 ± 0.002	4.525 ± 0.002	11	274	92
	PO	1.452 ± 0.020	2.837 ± 0.025	2	49	17
	PO <i>Swift</i>	0.975 ± 0.060	5.398 ± 0.083	85	355	221

Table 1. Parameter values (μ and σ) obtained by fitting a log–normal function (Eq. 7) to the distributions of θ_{jet} (Fig. 5, 6) and Γ_0 (Fig. 7) for all the simulated bursts (ALL), for those pointing to us (PO) and for those pointing to us and with a peak flux larger than P_{lim} , i.e. the *Swift* comparison sample (PO *Swift*). (*) fit of the distributions of GRBs pointing towards the Earth that should not have a jet break (see §5.2). For each distribution are reported the three moments: the mode, the mean and the median.

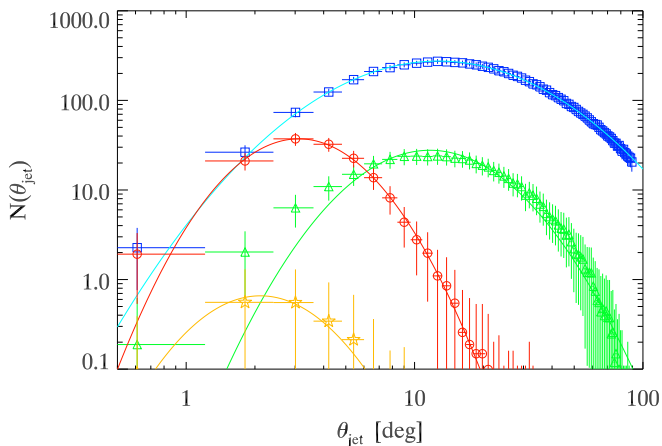


Figure 6. Distribution of θ_{jet} of GRBs: the PO simulated GRBs (open blue squares) and the GRBs of the PO class that have $\sin \theta_{\text{jet}} \leq 1/\Gamma_0$ (open green triangles) are shown. The latter are those that should not show any jet break time in their afterglow light curve. For the PO bursts with $P \geq 2.6 \text{ cm}^{-2} \text{ s}^{-1}$ (open red circles) we show the subsample of bursts that have $\sin \theta_{\text{jet}} \leq 1/\Gamma_0$ (open orange stars).

in GRBs is out of the scope of this paper, we notice that bursts with $\sin \theta_{\text{jet}} \leq 1/\Gamma_0$ can partly account for the explanation of the lack of measured jet breaks. This is the first time that such an argument is presented and surely deserves further studies.

Fig. 6 shows the distribution θ_{jet} of PO bursts (open blue squares) and the subsample of bursts with no jet break (open green triangles). These amount to $\sim 6\%$ of PO bursts. The mean of their log–normal distribution is $\theta_{\text{jet}} \sim 20^\circ$. One testable observational prediction of our simulations is that GRBs with no jet breaks should be preferentially soft (E_p^{obs} of few tens of keV). The open red circles in Fig. 6 correspond to PO bursts of the *Swift* comparison sample while the open orange star symbols correspond to bursts with no jet break. These have a mean jet opening angle $\sim 3.3^\circ$. We find that $\sim 2\%$ of the *Swift* bright bursts should not have jet break in their afterglow light curves. They could correspond to those events which do not show any evidence of a jet break in their optical light curve (e.g. Mundell et al. 2006; Grupe et al. 2007) although other observational selection effects very likely contribute to the paucity of the jet break measurements. The fit of the distributions shown in Fig. 6 with log–normal functions are reported in Tab. 1.

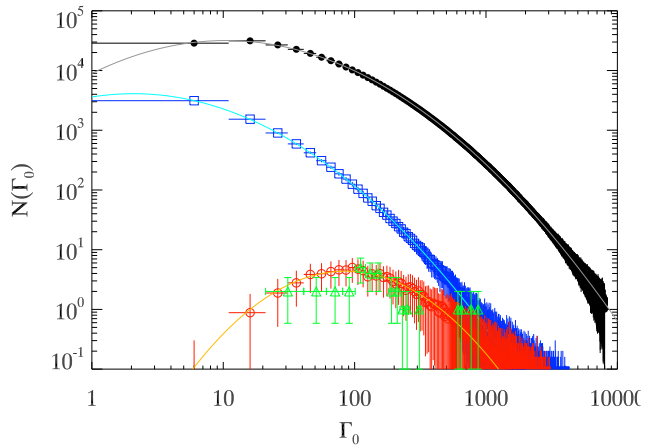


Figure 7. Distribution of Γ_0 of GRBs. Symbols as in Fig. 5. The 30 GRBs with Γ_0 estimated from the peak of their afterglow light curves (G12) are shown with the green open triangles.

4.6 Γ_0 distribution of GRBs

From our simulation we can derive the distribution of Γ_0 (Fig. 7). The total population of simulated bursts (filled circles in Fig. 7) has a log normal distribution with a mean $\Gamma_0 = 274$. Those pointing towards the Earth (open blue squares in Fig. 7) have a smaller mean, $\Gamma_0 = 49$. The PO bursts with peak flux larger than $2.6 \text{ cm}^{-2} \text{ s}^{-1}$, i.e. those of the *Swift* comparison sample, have a typical $\Gamma_0 = 355$. Although the distribution of Γ_0 factors for those bursts with a peak in their afterglow light curves (G12) is still made of few events, it agrees (open green triangles in Fig. 7) with that predicted by our simulations (for the sample of PO bursts of the *Swift* comparison sample – open red circles in Fig. 7).

Also in the case of Γ_0 we note that if we were able to measure Γ_0 for all the bursts that point towards the Earth, we would obtain a slightly smaller peak value of Γ_0 with respect to that of the distribution of all the bursts (pointing in every direction).

We note that the Γ_0 distribution of the general population of GRBs peaks at considerably low values of Γ_0 . This is a result of our simulations where, as explained in §4.2, we assume a peaked logarithmic distribution of Γ_0 with free peak and width. If we assume a distribution of Γ_0 with a smaller fraction of bursts with low Γ_0 –values, then we cannot reproduce the flux and fluence distributions

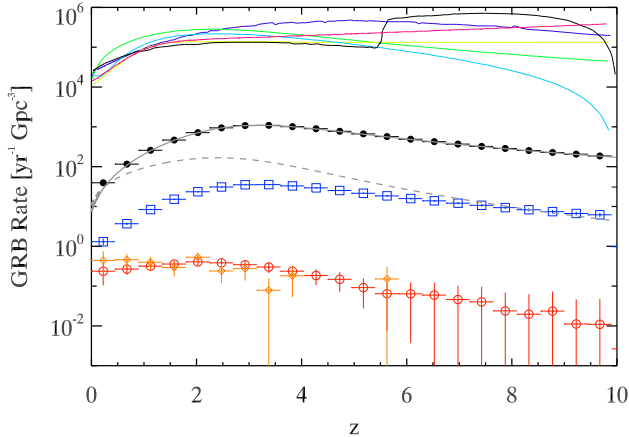


Figure 8. GRB rate as a function of redshift. The sample of simulated bursts is shown by the filled black circles and the GRB formation rate assumed in our simulation (see §2) is shown by the solid grey line. This curve is normalized to the histogram. The GRB formation rate without density evolution (as derived by Li et al. 2010 – see Eq. 1) is shown by the dashed grey line. The rate of bursts pointing to us (PO) is shown by the open (blue) squares and that of the PO bursts with $P \geq 2.6 \text{ cm}^{-2} \text{ s}^{-1}$ (i.e. the *Swift* comparison sample – PO *Swift*) by the open (red) circles. For comparison is also shown the rate of *Swift* GRBs of the complete sample (rescaled to match the rate of PO *Swift* rate). The solid lines reported in the top of the plot are the cosmic rates of SN Ib/c computed by Grieco et al. (2012) for different assumptions on the cosmic star formation rate.

and the detection rates of GRB detection of the GBM and BATSE instruments. Therefore, our simulations predict that a considerable fraction of GRBs should have Γ_0 as low as a few tens. These bursts might well be detected by current instruments. While the detailed study of their prompt and afterglow properties is out of the scope of the present paper, we note that their prompt emission should hardly differ from that of bursts with larger Γ_0 values (except for the obvious fact that their prompt E_p and L_{iso} is lower). In fact, if Γ_0 is low the fireball deceleration timescale (e.g. Eq. 14 in Ghirlanda et al. 2011) is $t_{\text{peak}} \sim 4 E_p^{1/3} \Gamma_{0,1}^{-8/3}$ hours which is much larger than the prompt emission timescale. So, while the prompt emission of low- Γ_0 burst should not be influenced by the afterglow contribution, their late time afterglow onset could be a distinctive feature (typical afterglow onset timescales are of the order of few hundreds second - Ghirlanda et al. 2011).

4.7 The GRB rate

Another consequence of our simulations is the rate of GRBs. This is shown as a function of redshift for the entire population of simulated bursts (filled circles in Fig. 8), in units of bursts $\text{Gpc}^{-3} \text{ yr}^{-1}$. The GRB redshift distribution (Eq. 1) assumed in our simulations is shown by the solid grey line in Fig. 8 and the observed star formation rate (Li 2008) is shown by the dashed (grey) line rescaled by an arbitrary factor to match the rate of GRBs at $z = 0$. We also show the rate of PO bursts (open blue squares) and that of the PO bursts of the *Swift* comparison sample (open red circles). Fig. 8 also shows the recent estimate of the rate of SN Ib/c computed by Grieco et al. (2012). The different curves for SN Ib/c correspond to different assumption of the cosmic star formation rate (CSFR) in that paper. As a result of our simulation, the local rate of GRBs is $\sim 0.3\%$ that of SN Ib/c.

5 SUMMARY AND DISCUSSION

We have studied two fundamental parameters of GRBs: the jet opening angle θ_{jet} and the bulk Lorentz factor Γ_0 . The first question that we aimed to answer was *whether θ_{jet} and Γ_0 have preferential values*. The direct measure of θ_{jet} through the jet break times observed in the optical light curves (Frail et al. 2001; Ghirlanda et al. 2004, 2007) shows that $\theta_{\text{jet}} \sim 5^\circ$. The measure of Γ_0 from the peak of the afterglow light curve for ~ 30 GRBs (G12) also shows a characteristic value⁸ of $\Gamma_0 \sim 60$. However, the limited number of events with a direct estimate of θ_{jet} and Γ_0 and the possible selection effects, related to the difficulties of measuring these two parameters (see §1), prevent us to assume them as representative of the GRB population. In particular we want to test the consistency of different possible distributions of θ_{jet} and Γ_0 with a set of available observational constraints (§2). Moreover, we aim at constraining the free parameters of the distributions of θ_{jet} and Γ_0 and derive if and how these two parameters are correlated.

In this paper we used a population synthesis code to simulate GRBs with different assigned distributions of θ_{jet} and of Γ_0 each one with a set of free parameters that we left free to vary within certain ranges. Obviously, we did not assume the observed distributions of θ_{jet} and Γ_0 as constraints to avoid circularity.

We assume that GRBs have a unique comoving frame peak energy E'_p and collimation-corrected energy E'_γ (the large black dot in Fig. 1) which are transformed into their corresponding rest frame E_p and E_γ respectively. The assigned θ_{jet} and Γ_0 allow us to derive the isotropic equivalent energy of the simulated bursts according to the relative value of θ_{jet} and Γ_0 . $E_{\text{iso}} \sim E_\gamma / \theta_{\text{jet}}^2$ if $\sin \theta_{\text{jet}} > 1/\Gamma_0$, while $E_{\text{iso}} \sim E_\gamma \Gamma_0^2$ in the opposite case. This introduces a “natural bias” in the distribution of E_{iso} : those bursts with a small enough Γ_0 will have an isotropic energy which is smaller than that one would calculate using the value of θ_{jet} . In the $E_p - E_{\text{iso}}$ plane of Fig. 1 this corresponds to a limit $E_p \propto E_{\text{iso}}^{1/3}$. Bursts with $1/\Gamma_0 > \sin \theta_{\text{jet}}$ will lie along this limiting line and there should be no GRBs on the right of this line [i.e. in region (III) in Fig. 1].

This is the first time that the limit mentioned above is considered within the framework of studying the distributions of GRBs in e.g. the $E_p - E_{\text{iso}}$ plane. Indeed, this limiting line can account for the absence, in the observed GRB sample with measured z and well constrained peak energy (i.e. the bursts used to construct the $E_p - E_{\text{iso}}$ correlation), of bursts with intermediate/low peak energy E_p and very large E_{iso} .

The assumed distributions of Γ_0 and θ_{jet} determine the distribution of simulated bursts in the $E_p - E_{\text{iso}}$ plane of Fig. 1. We considered two types of distributions for θ_{jet} and Γ_0 : (A) a power law distribution, i.e. θ_{jet} and Γ_0 do not assume any preferential value or (B) both θ_{jet} and Γ_0 have peaked distributions (either broken power law or a log-normal distributions).

In order to test these two hypothesis we compared the results of our simulations with three GRB samples: the complete *Swift* sample of GRBs detected by BAT with measured redshifts (S12), the sample of bursts detected by the GBM in the last 2 years (Goldstein et al. 2012) and the 4th BATSE catalog of GRBs (Meegan et al. 1997). The simulations should reproduce several proprieties of these samples.

While most of the bright bursts of the *Swift* complete sample of S12 have measured z and provide an observational constrain in

⁸ This average value is obtained assuming that the circumburst medium has a wind density profile (see G12).

the rest frame $E_p - E_{\text{iso}}$ and observer frame $E_{\text{peak}}^{\text{obs}} - F$ plane (left and right panels of Fig. 2,3,4, respectively), the number count distribution and rate of the BATSE and GBM populations of bursts (mostly without measured z) are used as additional constraints since they map the faint end of the number count distribution of GRBs.

Our main result is that we cannot reproduce all our observational constraints if the Γ_0 and θ_{jet} distributions are power laws. In this case the rate of GBM and BATSE bursts predicted by our simulations is a factor ~ 2 larger than the real one and the distribution of the *Swift* simulated bursts in the $E_p - E_{\text{iso}}$ and $E_{\text{peak}}^{\text{obs}} - F$ plane is inconsistent with the real complete sample of *Swift* bursts.

Instead, if θ_{jet} and Γ_0 have broken power law distributions (with peak values $\theta_{\text{jet}} \sim 4.5^\circ$ and $\Gamma_0 \sim 70$) or log-normal distributions (with peak values $\theta_{\text{jet}} \sim 4.5^\circ$ and $\Gamma_0 \sim 85$) a better agreement between the simulations and the observational constraints is found. However, the broken power law or log-normal case produce a linear $E_p - E_{\text{iso}}$ correlation due to the assumption that the simulated bursts have a θ_{jet} distribution with a unique peak value (see §4). This motivated us to consider the possibility that there is a relation between the peak values of the distributions of θ_{jet} and Γ_0 . G12 found that among GRBs with a Γ_0 estimate, three new correlations are found: $E_{\text{iso}} \propto \Gamma_0^2$, $L_{\text{iso}} \propto \Gamma_0^2$ and $E_p \propto \Gamma_0$. The combination of these correlations with the assumptions that $\theta_{\text{iso}}^2 \Gamma_0 = \text{const}$ allows to derive the three main empirical correlations of GRBs: the $E_p - E_{\text{iso}}$ correlation, the $E_p - L_{\text{iso}}$ correlation and the $E_p - E_\gamma$ correlation.

We therefore assumed that both θ_{jet} and Γ_0 have log-normal distributions and that a relation of the type $\theta_{\text{jet}}^m \Gamma_0 = \text{const}$ exists between the peak values of their respective log-normal distributions. We found good consistency between our simulations and the observational constraints (Fig. 4) in the case of a log-normal distribution of Γ_0 with central value 90 and logarithmic dispersion of 0.65. The distribution of θ_{jet} (also a log-normal) is in this case determined by the relation $\theta_{\text{jet}}^m \Gamma_0 = \text{const}$ which we find should have $m = 2.5$. This value is what one obtains by combining the above scaling relations (between Γ_0 and E_{iso} , E_p) with the $E_p - E_{\text{iso}}$ correlation of the *Swift* complete sample which is $E_p \propto E_{\text{iso}}^{0.6}$. The existence of a relation $\theta_{\text{jet}}^m \Gamma_0 = \text{const}$ (with $m \sim 1$ and $\text{const} = 10-40$) is also predicted from recent models of magnetically accelerated jets in GRBs (e.g. Tchekhovskoy et al. 2011).

We found that the Γ_0 distribution that best reproduces all our observational constraints extends to low Γ_0 values. If we cut the Γ_0 distribution so to exclude such low values of Γ_0 we cannot reproduce the observed flux and fluence distributions and detection rates of BATSE and GBM. Therefore, we find that low- Γ_0 bursts should exist in populations of GRBs detected by most sensitive detectors. Although a detailed study of the prompt and afterglow properties of these events is out of the scopes of this paper, we can draw some remarks. Apart from their relatively low E_p and L_{iso} (which are correlated with Γ_0 as found by G11), the low- Γ_0 bursts should have a late time afterglow onset (i.e. a few hours for typical parameters, see §4.6). Therefore, their prompt emission should not be contaminated by the afterglow while their late time afterglow onset could be one of their distinctive features.

An immediate consequence of our results is that the large scatter of the $E_p - E_{\text{iso}}$ correlation can be interpreted as due to the jet opening angle distribution of GRBs. The found inverse relation between θ_{jet} and Γ_0 implies that bursts with the largest bulk Lorentz factors should have a smaller average θ_{jet} . On the other hand, bursts with relatively low average Γ_0 factors should also have, on average, large θ_{jet} .

Our results depend on the assumption that all bursts have the

same $E'_p = 1.5$ keV and $E'_\gamma = 1.5 \times 10^{48}$ erg. Although there could be a dispersion of these values, our results still hold if the width of this dispersion is not larger than the dispersion of the observed quantities. We note that larger values of E'_p and E'_γ would move the $E_p \propto E_{\text{iso}}^{1/3}$ (Eq. 6) towards the upper part of the plane of Fig. 1. As a consequence some of the real GRBs of the *Swift* complete sample, would be cut out of the plane because they would lie in the forbidden region (III) of this plane. On the other side we could assume lower values of E'_p and E'_γ . Since we do not know their real dispersion, we tried to assume $E'_p = 0.15$ keV and $E'_\gamma = 1.5 \times 10^{47}$ (i.e. a factor 10 lower than the values assumed in the simulation). Under this different assumption, for the case of log-normal distributions of both θ_{jet} and Γ_0 and of an intrinsic relation between these two parameters, we find that the θ_{jet} distribution is consistent with that found with the fiducial values of E'_p and E'_γ , but with a different distribution of Γ_0 . Indeed, in this case we find a mean value $\Gamma_0 \sim$ a factor 3 larger than that of the present simulation. Although it is not possible at the present stage to constrain the distribution of E'_p and E'_γ , these results suggest that their dispersion should be lower than a factor of ~ 10 .

Our best simulations allow us to derive the properties of three populations of GRBs: those that are pointing to us and that have a peak flux bright enough to enter in the *Swift* bright sample (i.e. with the same peak flux threshold adopted for the *Swift* complete sample of S12), those that are pointing to us and, finally the full population of simulated GRBs, oriented randomly in the Universe (i.e. pointing to us and not). The latter is the GRB population that we cannot study on the base of the bursts that we detect. The main advantage of our population synthesis code is that we can infer the properties (e.g. the Γ_0 and θ_{jet} distribution and the true GRB rate in this work) of this population of bursts, which is inaccessible through the observations.

One immediate consequence of our simulation is the true $E_p - E_{\text{iso}}$ correlation. If we consider the PO bursts and if we were in principle able to detect them all, we should find a different $E_p - E_{\text{iso}}$ correlation than the one presently reported in the literature. Indeed, the fit of the PO bursts in the $E_p - E_{\text{iso}}$ plane of Fig. 4 yields a correlation with slope 0.5 and normalization -27.6 while the entire GRB population, the total simulated bursts, have a $E_p - E_{\text{iso}}$ correlation with slope 0.44 and normalization -20.7. This is due to the fact that PO bursts tend to populate the lower region of the $E_p - E_{\text{iso}}$ plane (Fig.4) where the $E_{\text{iso}}^{1/3}$ limit cuts their distribution in the $E_p - E_{\text{iso}}$ plane. Therefore, if we could measure E_{iso} and E_p for all the bursts that point to us, we should determine a flatter $E_p - E_{\text{iso}}$ correlation than that observed so far in the high part of the plane with bright bursts.

Our simulation predicts that the bright bursts detected by *Swift* should have a mean opening angle of $\theta_{\text{jet}} \sim 4.7^\circ$. This value is only a factor 2 smaller than the mean of the entire GRB population that we have simulated (which has $\theta_{\text{jet}} \sim 8.7^\circ$). However, from Fig. 5 (open blue squares) one can see that if we were able to detect fainter GRBs and to measure their jet opening angle, we would obtain a mean of 40° . Intriguingly we note that the present distribution of θ_{jet} measured from the optical afterglow break times in a few bursts is representative of the θ_{jet} distribution of the entire population of bursts. This is because the bursts that we have detected so far populate the high region of the $E_p - E_{\text{iso}}$ plane where the θ_{jet} distribution can be almost unbiasedly sampled. In fact, only the bursts at lower values of E_p and E_{iso} are affected by the ‘‘natural bias’’ of $1/\Gamma_0 > \sin\theta_{\text{jet}}$. The low E_p - low E_{iso} region is where PO

bursts concentrate (they have large θ_{jet} or small Γ_0 , enhancing the probability to point at us).

Our simulation predicts that there are bursts with no jet break, the ones with $1/\Gamma_0 > \sin\theta_{\text{jet}}$. Their afterglows will never have a jet break since the condition $1/\Gamma_0 \sim \sin\theta_{\text{jet}}$ is never met but their afterglow light curve should have a characteristic post-jet break intermediate/steep decay slope. These should be $\sim 6\%$ of the bursts pointing to us and $\sim 2\%$ of the bursts detected by *Swift* with $P > P_{\text{lim}}$.

According to our best simulation, the mean Γ_0 of all bursts is $\langle \Gamma_0 \rangle = 274$. The Γ_0 distribution is highly asymmetric and there is a considerable difference between its mode (i.e. the peak) the mean and the median. The simulated bursts pointing to us corresponding to the *Swift* complete sample have $\langle \Gamma_0 \rangle = 355$. These two values are broadly consistent, as explained above, since these bursts populate the upper part of the $E_p - E_{\text{iso}}$ plane where the distribution of GRBs is almost free from the “natural bias”. Remarkably, if we were able to measure Γ_0 for all the bursts pointing to us, we would find a very low value of the mean of $\langle \Gamma_0 \rangle = 50$. Finally, we have found that the distribution of Γ_0 that we predict for the *Swift* bright sample is consistent with the distribution of Γ_0 of the GRBs studied in G12.

We can derive from our simulations the true rate of GRBs. Previous studies of the GRB rate assumed a unique value of θ_{jet} , typically 0.2 rad or the *observed* distribution of θ_{jet} (e.g. Guetta et al. 2005; Grieco et al. 2012). Our simulations (§4.5) show that the peak of the intrinsic/global distribution of θ_{jet} is a factor 2 larger than the real intrinsic distribution and has a much wider dispersion (Tab.1). Differently from existing GRB rate estimates based on the correction of the isotropic GRB rate for an *average* beaming factor (e.g. Guetta et al. 2005; Grieco et al. 2012) in our simulation the total number of simulated bursts is adjusted in order to reproduce the rate of detections of GBM and BATSE. Therefore, we have the rate of GRBs as a function of redshift independently from the value of θ_{jet} of each single burst. If we compare this rate with that of SNIb/c (from Gireco et al. 2012) we find that the local rate of GRBs is $\sim 0.3\%$. Moreover, if we consider the 7% fraction of SNIb/c which produce Hypernovae events (Guetta & Della Valle 2007) we find that the rate about 4.3% of local Hypernovae should produce a GRB.

ACKNOWLEDGMENTS

We thank the referee for comments and suggestions that improved the manuscript. We acknowledge ASI I/004/11/0 and the 2011 PRIN-INAF grant for financial support.

REFERENCES

Amati, L., Frontera, F., Tavani, M. et al. 2002, A&A, 390, 81
 Amati, L., Frontera, F., & Guidorzi, C. 2009, A&A, 508, 173
 Band, D., Matteson, J., Ford, L. et al. 1993, ApJ, 413, 281
 Band, D. L., & Preece, R. 2005, ApJ, 627, 319
 Barbiellini, G., Longo, F., Omodei, N., et al. 2006, NCimB, 121, 1363
 Bosnjak, Z., Celotti, A., Longo, F., Barbiellini, G., 2008, MNRAS, 384, 599
 Burrows D. N., Romano P., Falcone A., et al. 2005, Sci, 309, 1833
 Butler, N. R., Kocevski, D., Bloom, J. S., & Curtis, J. L. 2007, ApJ, 671, 656
 Butler, N. R., Kocevski, D., & Bloom, J. S. 2009, ApJ, 694, 76
 Collazzi A. C., Schaefer B. E., Goldstein A., Preece R. D., 2012, ApJ, 747, 39

Dado S., Dar A., De Rujula A., 2007, ApJ, 663, 400
 Eichler, D., & Levinson, A. 2005, ApJ, 635, 1182
 Falcone A. D., Morris D., Racusin J., et al., 2007, ApJ, 671, 1921
 Firmani C., Ghisellini G., Ghirlanda G., Avila-Reese V., 2005, MNRAS, 360, L1
 Firmani C., Cabrera J.I., Avila-Reese V., Ghisellini G., Ghirlanda G., et al., 2009, MNRAS, 393, 1209
 Frail D. A., Kulkarni S. R., Sari R., et al, 2001, ApJ, 526, L55
 Ghirlanda, G., Ghisellini, G., Lazzati, D. 2004, ApJ, 616, 331
 Ghirlanda, G., Ghisellini, G., Firmani, C. 2005, MNRAS, 361, L10
 Ghirlanda, G., Nava, L., Ghisellini, G., Firmani, C., Cabrera, J. I., 2008, MNRAS, 387, 319
 Ghirlanda G., Nava L., Ghisellini G., Firmani C., 2007, A&A, 466, 127
 Ghirlanda, G.; Nava, L.; Ghisellini, G.; Celotti, A.; Firmani, C., 2009, A&A, 496, 585
 Ghirlanda, G., Nava, L.; Ghisellini G., 2010, A&A, 511, 43
 Ghirlanda, G., Ghisellini G., Nava, L., 2011, MNRAS, 418, L109
 Ghirlanda, G., Ghisellini G., Nava, L., 2011a, MNRAS, 410, L97
 Ghirlanda, G., Nava, L.; Ghisellini G., et al., 2012, MNRAS, 420, 483 (G12)
 Ghirlanda, G. Ghisellini G., Nava, L. et al., 2012b, MNRAS, 422, 2553
 Ghisellini G., Nardini M., Ghirlanda G., Celotti A., 2009, MNRAS, 393, 253
 Ghisellini G., Ghirlanda G., Nava L., Celotti A., 2010, MNRAS, 403, 926
 Giannios, D., & Spruit, H. C. 2007, A&A, 469, 1
 Giannios, D., 2012, MNRAS, 422, 3092
 Goldstein A., Burgess J. M., Preece R. D., et al., 2012, ApJS, 199, 19
 Grieco V., et al., 2012, MNRAS in press, arXiv:1204.2417
 Grupe D., Gronwall C.; Wang X.-Y., et al., 2007, ApJ, 662, 443
 Guetta D., Piran T., Waxman E., 2005, ApJ, 619, 412
 Guetta D. & Della Valle M., 2007, A&A, 461, 95
 Hopkins A. M., Beacom J. F., 2006, ApJ, 651, 142
 Kaneko, Y., Preece, R. D., Briggs, M. S. et al. 2006, ApJS, 166, 298
 Kocevski D. & Butler N., 2008, ApJ, 680, 531
 Kocevski, D., 2012, ApJ, 747, 146
 Komissarov S. S., Vlahakis N., Koenigl A., 2010, MNRAS, 407, 17
 Krimm, H. A., Yamaoka, K., Sugita, S., et al. 2009, ApJ, 704, 1405
 Lamb, D. Q., Donaghy, T. Q., & Graziani, C. 2005, ApJ, 620, 355
 Lazzati D., Morsony B. J. & Begelman M. C., 2011, ApJ, 732, 34
 Leninson, A., & Eichler, D. 2005, ApJ, 629, L13
 Li, Li-Xin, 2008, MNRAS, 388, 1487
 Meegan C. A., Paciesas W. S., Pendleton G. N., et al., 1998, AIPC, 428, 3
 Mundell C. G., Melandri A., Guidorzi C., et al., 2007, ApJ, 660, 489
 Nakar, E. & Piran, T. 2005, MNRAS, 360, L73
 Nava L., Ghisellini G., Ghirlanda G., et al., 2006, 450, 471
 Nava, L., Ghirlanda, G., Ghisellini, G., Firmani, C. 2008, MNRAS, 391, 639
 Nava, L., Ghirlanda, G., Ghisellini, G. et al., 2011a, A&A, 530, 21
 Nava, L., Ghirlanda, G.; Ghisellini, G.; Celotti, A., 2011b, MNRAS, 415, 3153
 Nava, L., Salvaterra, R., Ghirlanda, G., et al., 2012 (N12), MNRAS, 421, 1256
 Paciesas W. S., Meegan C. A., von Kienlin A., et al., 2012, ApJS, 199, 18
 Panaitescu A., & Kumar P., 2001, ApJ, 560, L49
 Panaitescu A., 2009, MNRAS, 393, 1010
 Piran, T., 1999, PhR, 314, 575
 Racusin J. L., Liang E. W., Burrows D. N., et al., 2009, ApJ, 698, 43
 Rees, M., & Meszaros, P. 2005, ApJ, 628, 847
 Ryde, F., Bjornsson, C., Kaneko, Y., et al. 2006, ApJ, 652, 1400
 Sakamoto T., Barthelmy S. D., Baumgartner W. H., et al., 2011, ApJS, 195, 2
 Salvaterra R., Campana S., Vergani S. D., et al., 2012, ApJ, 749, 68
 Shahmoradi A., & Nemiroff R. J., 2011, MNRAS, 411, 1843
 Soderberg A. M., Kulkarni S. R., Nakar E., et al., 2006, Nature, 422, 1014
 Toma, K., Yamazaki, R., & Nakamura, T. 2005, ApJ, 635, 481
 Tchekhovskoy A., McKinney J. C., Narayan R., 2009, ApJ, 699, 1789
 Thompson, C. 2006, ApJ, 651, 333
 Thompson, C., Meszaros, P., & Rees M. J. 2007, ApJ, 666, 1012
 Van Eerten, H., Zhang, W., MacFadyen A., 2010, ApJ, 772, 235

- Van Eerten, H., Meliani, Z., Wijers, R. A. M., Kippens, R., 2011, MNRAS, 410, 2016
Yamazaki, R., Ioka, K., & Nakamura, T. 2004, ApJ, 606, L33
Yonetoku, D., Murakami, T., Nakamura, T. et al. 2004, ApJ, 609, 935